Nanoscale

Ultrasmall Au nanocatalysts supported on nitrided carbon for electrocatalytic CO2 reduction: the role of carbon support in high selectivity

Journal:	*Nanoscale*
Manuscript ID	NR-ART-05-2018-004322.R1
Article Type:	Paper
Date Submitted by the Author:	05-Jul-2018
Complete List of Authors:	Jin, Lei; University of Connecticut, Department of Chemistry Liu, Ben; Nanjing Normal University, Chemistry and Materials Science Wang, Pu; Xiangtan University, Chemistry Yao, Huiqin; University of Connecticut, Department of Chemistry Achola, Laura; University of Connecticut, Department of Chemistry Kerns, Peter; University of Connecticut, Department of Chemistry Lopes, Aaron ; Department of Chemsitry Yang, Yue; University of Connecticut, Department of Chemistry Ho, Josha; University of Saskatchewan College of Arts and Science, Physics and Engineering Physics Moewes, Alexander; University of Saskatchewan, Physics and Engineering Physics Pei, Yong; Xiangtan University, Chemistry He, Jie; University of Connecticut, Department of Chemistry

Nanoscale

ARTICLE

Ultrasmall Au nanocatalysts supported on nitrided carbon for electrocatalytic CO_2 reduction: the role of carbon support in high selectivity

Received 00th January 20xx,
Accepted 00th January 20xx

DOI: 10.1039/x0xx00000x

www.rsc.org/

Lei Jin,[a] Ben Liu,[a,c] Pu Wang,[d] Huiqin Yao,[a,e] Laura A. Achola,[a] Peter Kerns,[a] Aaron Lopes,[a] Yue Yang,[a] Josha Ho,[f] Alexander Moewes,[f] Yong Pei,[d] and Jie He*[a,b]

Au is one of the most promising electrocatalysts to convert CO_2 to CO in an aqueous-phase electrochemical reduction. However, ultrasmall Au nanocatalysts (AuNCs, < 2 nm) have proven to be favorable for water reduction over CO_2, although they possess a large surface-to-volume ratio and potentially are ideal for CO_2 reduction. We herein report that ultrasmall AuNCs (1.9 ± 0.3 nm) supported on nitrided carbon are remarkably active and selective for CO_2 reduction. The mass activity for CO of AuNCs reaches 967 A g^{-1} with a Faradaic efficiency for CO of ~83% at -0.73 V that is an order of magnitude more active than the state-of-the-art results. The high activity is endowed by the large surface area per unit weight and the high selectivity of ultrasmall AuNCs for CO_2 reduction is originated from the cooperative effect of Au and the nitrided carbon support where the surface N sites act as Lewis bases to increase the surface charge density of AuNCs and enhance the localized concentration of CO_2 nearby catalytically active Au sites. We show that our results can be applied to other pre-synthesized Au catalysts to largely improve their selectivity for CO_2 reduction by 50%. Our method is expected to illustrate a general guideline to effectively lower the cost of Au catalysts per unit weight of the product while maintaining its high selectivity for CO_2 reduction.

Introduction

Efficient and selective conversion of CO_2 to useful chemicals and fuels has received considerable attention as a mean to reduce CO_2 emission known as an increasing environmental threat.[1-8] The key for various CO_2 conversions is to develop new catalysts.[9] Au nanocatalysts (AuNCs), among various metal catalysts developed so far,[10-15] show high activity to convert CO_2 to CO in aqueous-phase electrochemical reduction.[16-28] Despite many advances and successful examples of electrocatalytic CO_2 reduction, there are two unmet challenges that have largely limited the industrial use of Au catalysts for CO_2 electroreduction. On one hand, poor selectivity (or low Faradaic efficiency, FE) of CO_2/CO is often received, arising from the competitive reduction of H_2O/H_2. The standard potential of CO_2/CO is -0.106 V (*vs.* reversible hydrogen electrode (RHE), all potentials reported here are with respective to RHE), which is more difficult to be reduced thermodynamically compared to H_2O/H_2.[5, 29] The groups of Cuenya[30] and Jin[24] showed that AuNCs having sub-2 nm in diameter catalyzed electrocatalytic CO_2 reduction to CO even at very low overpotentials (η, *e.g.*, < 100 mV for Au_{25} nanoclusters) but the FE for CO_2 reduction was <20% at η = 550 mV. Although the reduction operating at high η receives higher FE to CO,[24] it needs much greater energy input.

On the other hand, high cost of the catalyst per unit weight of the product (*i.e.* CO) has largely limited the commercialization of Au catalysts for CO_2 electroreduction. The groups of Sun[22] and Bao[26] demonstrated that AuNCs in the size range of 2-10 nm exhibited mass activity of < 20 A per g_{Au} toward the formation of CO at η = 550 mV.[19, 22, 26] In order to lower the cost of the catalyst per unit weight of the product, an important factor is to reduce the size of Au that increases the proportion of surface atoms and maximizes the usage of all Au atoms. However, AuNCs having smaller sizes have proven to be more favorable for water reduction.[22, 24, 30, 31]

To solve those challenges in CO_2 reduction, enhancing the favorable interaction of CO_2 to catalysts over H_2O is essential. One way to improve the binding of electrophilic CO_2 to AuNCs is to vary surface charge density of Au catalysts.[26, 27] For example, the use of carbene as surface ligands to modify Au nanoparticles (NPs) was demonstrated to enrich the surface charge of Au by the groups of Yang and Chang,[27] because of the σ donation from carbene ligands. Carbene-modified Au

[a] Department of Chemistry, University of Connecticut, Storrs, CT 06269, USA. E-mail: jie.he@uconn.edu
[b] Institute of Material Science, University of Connecticut, Storrs, CT 06269, USA.
[c] Jiangsu Key Laboratory of New Power Batteries, Jiangsu Collaborative Innovation Center of Biomedical Functional Materials, School of Chemistry and Materials Science, Nanjing Normal University, Nanjing 210023, China
[d] Department of Chemistry, Key Laboratory of Environmentally Friendly Chemistry and Applications of Ministry of Education, Xiangtan University, Hunan 411105, China
[e] Department of Chemistry, NingXia Medical University, Yinchuan 750004, China
[f] Department of Physics and Engineering Physics, University of Saskatchewan, 116 Science Place, Saskatoon, Saskatchewan S7N 5E2, Canada

Electronic Supplementary Information (ESI) available: [details of any supplementary information available should be included here]. See DOI: 10.1039/x0xx00000x

facilitated CO_2 binding with significantly enhanced CO FE over hydrogen production. Our group recently reported the *in situ* growth of ligand-free, sub-2 nm AuNCs onto virtually any carbon supports using a facile and environmental friendly "soft nitriding" technique.[32-34] Those AuNCs are ultrasmall in size with a large proportion of surface atoms (> 60%, edge/corner atoms predominantly). Nitrogen-rich carbon supports showed strong electronic interaction with Au where N sites enriched the surface charge density of Au.[32] Such electron-rich AuNCs with high surface area are therefore hypothesized to enhance the efficiency for CO_2 binding and reduction, in spite of the ultrasmall size of AuNCs, as confirmed by density functional theory (DFT) calculation. Moreover, we envision that N sites on the surface of carbon supports act as basic sites to potentially increase the localized concentration of CO_2 nearby catalytically active Au.[35-37] This in turn shifts the binding equilibrium of CO_2 to Au according to the Le Chatelier's principle.[38, 39] AuNCs supported on nitrided carbon (AuNCs@CN) thus favor the electroreduction of CO_2. At η = ~544 mV, AuNCs@CN show a mass activity of 714 A g^{-1} with CO FE of 89% (Figure 1), that is an order of magnitude more active (with high selectivity as well) than the state-of-the-art results.[19, 22, 26] One of the attractive features is the possibility to use nitrided carbon to support other pre-synthesized AuNCs which are *ca.* 50% more active for CO_2 reduction, compared to the same AuNCs on pristine carbon.

Experimental

Materials

$HAuCl_4$, urea, $NaBH_4$, hydrochloric acid (HCl), sodium hydroxide, nafion (5 wt% solution in alcohol), chloroform, 1-chloroethanol, potassium iodide, oleylamine, 4-mercaptobenzoic acid (MBA), ascorbic acid (AA), ethanol, and hexane were all purchased form Sigma-Aldrich and used without further purification. Printex U activated carbon was kindly provided by Orion. Deionized water (High-Q, Inc. 103S Stills) with a resistivity of > 10.0 MΩ was used in experiments.

Synthesis of Au-2@CN, Au-5@CN, and Au-8@CN

Au-2@CN was synthesized by following our previous report.[32-34] Briefly, the activated carbon (2 g) was mixed with urea (3 g). This mixture was sealed in a crucible using aluminum foil, followed by annealed at 150 °C for 2 h and 300 °C for 2 h. The nitrided carbon (CN) was collected after washing with water and ethanol three times and dried at 60 °C under vacuum. To prepare Au-2@CN, 100 mg of CN was first dispersed in 200 mL of water by sonicating for 1 h at *r.t.* 5 mg of $HAuCl_4$ was added to the above mixture, followed by stirring for 2 h. Then, 6 mL of freshly prepared $NaBH_4$ solution (ice-cooled, 1 mg/mL) was added. After stirring for 1h, Au-2@CN was collected by washing with water and ethanol, followed by drying at 60 °C. Au-5@CN was prepared by growing the Au on CN in the reaction solution with pH = 3, tuned by adding HCl solution. The Au-8@CN was prepared by growing the Au on CN in the reaction solution with pH=12, tuned by adding NaOH solution.

Synthesis of AuNCs using Au-2@CN as seed

Au with different sizes on CN was also synthesized via a seed-growth method using Au-2@CN.[40] The size of Au can be tuned via the feeding amount of $HAuCl_4$. Taking Au-2.9 nm as an example, 20 mg of Au-2@CN was first dispersed in 16.4 mL of ethanol/water solution (ethanol : water = 3:1 by volume). Then, 1.95 mL of MBA (0.436 mg/mL in ethanol) and 75 uL of $HAuCl_4$ (10 mg/mL in water) was added into above solution, followed by adding 976 uL of AA (7.37 mg/mL in ethanol/water). After stirring 1 min, the solution was aged overnight. The sample was washed with ethanol twice before drying in the oven at 60 °C. The resulting power was further annealed at 250 °C in the air for 1 h to remove surface ligands.

Synthesis of physically adsorbed Au on CN and C

Oleylamine-modified AuNPs were synthesized by following the previous report.[41, 42] Firstly, $HAuCl_4$ $3H_2O$ (0.5 mmol) was dissolved in the mixture of oleylamine (2 mL) and hexane (20 mL) in a round bottom flask at room temperature. 1 mmol of *tert*-butylamine borane complex was dissolved in 2 mL of oleylamine and 2 mL of hexane simultaneously. The *tert*-butylamine borane solution was injected into the precursor solution in the round bottom flask. After stirring for one hour at room temperature, ethanol was added to the solution to precipitate the Au NPs, followed by centrifugation to collect the Au NPs. The Au NPs were re-dispersed in hexane to form 1 mg mL^{-1} solution for the further usage.

The physically adsorbed Au on CN and C was prepared by following the previous report.[22] Typically, 50 mg of CN (or C) was dispersed in 20 mL hexane by sonification. Then the 1.25 mL Au solution (1 mg mL^{-1}) was added into the CN suspension, followed by stirring in the fume hood overnight to evaporate the solvent. The resulted power was further annealed at 180 °C in the air overnight to remove the surface ligand.

Synthesis of chloroform quenched Au-2@CN (Au-2@QCN1) and chloroethanol quenched Au-2@CN (Au-2@QCN2)

We used two different methods to quench surface N sites. Au-2@QCN1 was prepared using chloroform as the quenching agent. Briefly, 10 mg of Au-2@CN was dispersed in 5 mL of 0.5 M NaOH solution and 5 mL of ethanol by sonication. Then 2 mg of chloroform was added into the solution, followed by keeping the reaction at 60 °C overnight. The sample was washed with H_2O and ethanol, followed by drying in the oven at 60 °C. Au-2@QCN2 was prepared using chloroethanol as the quenching agent. Briefly, 10 mg of Au-2@CN was dispersed in 5 mL of 0.5 M NaOH solution and 5 mL of ethanol by sonication. Then 5 mg of chloroethanol and 1 mg of KI was added into the solution, followed by keeping the reaction at 60 °C overnight. The sample was washed with H_2O and Ethanol, followed by drying in the oven at 60 °C. The similar quenching experiments

were carried out for CN to give QCN1 and QCN2 for XAS measurements.

Electrochemical measurements

A CH Instruments 627E workstation was used for all CO_2 reduction. Pt wire and SCE were used as the counter electrode and the reference electrode, respectively. The working electrode is a pyrolytic graphite (PG) electrode coated with the ink of catalysts. Typical, Au catalysts (2 mg) was dispersed in 380 uL of water, 95 uL of ethanol, and 25 uL of Nafion solution to get the uniform ink. 10 uL of Au catalyst ink was dropped on the PG electrode and dried at room temperature before using. Linear sweep voltammetry (LSV) scans were carried out in 0.5 M $NaHCO_3$ solution in the potential window of -0.5 V to -1.7 V (*vs* SCE) at the scan rate of 10 mV s^{-1}. The electrolyte solution was saturated with N_2 or CO_2 before any tests and the potential were converted to RHE using the equation below:

$$E(RHE) = E(SCE) + 0.244V + 0.0591 \times pH$$

The pH was 7.2 and 8.4 when the electrolyte was saturated with CO_2 and N_2, respectively. The mass activity of catalysts was calculated based on the following equation:

$$j_{CO} = \frac{i \times FE}{m} \qquad (1)$$

where the *i*, FE, and m are the current, Faradaic efficiency at specific potential, and the loading mass of Au on the electrode, respectively.

The electrochemical surface area was estimated from the reduction peak of Au catalysts in the electrolyte of 0.1 M $HClO_4$[23]. The electrode was first scanned from 0.26 V to 1.66 V at a scan rate of 50 mV/s to oxidize the Au surface. Then, the oxidized Au was reduced with the scan from 1.66 V back to 0.26 V. The reduction peak of Au was used to calculate the electrochemical surface area as described previously. 390 μC/cm^2 was used as the reference charge value for Au[43]. The equation to calculate the ECSA was shown below:

$$Charge = \frac{Area\ of\ Au\ reduction\ peak}{Scan\ rate} \qquad (2)$$

$$ECSA = \frac{Charge}{390\ \mu C/cm^2} \qquad (3)$$

Products analysis

The electrochemical CO_2 reduction experiments were carried out in a customized H-cell with separated cathode and anode by a frit bridge (Figure S1). The working electrode and reference electrode are sealed in one part and the counter electrode was in the other part. SCE and Pt wire were used as reference electrode and counter electrode in all experiments and the potentials were all converted to RHE. 0.5 M $NaHCO_3$ was used as the electrolyte in all experiments. 20 mL of electrolyte was added into both cells, leaving 13 mL of head space. The electrolyte was bubbled with CO_2 for at least 20 mins before tests. I-t curve was measured at different potentials and the products at different potentials were analyzed using gas chromatography. The amount of products (H_2 and CO) was calculated from the peak area using the standard calibration curves.

Characterizations

TEM and HR-TEM were carried on a JEOL 2010 transmission electron microscope with an accelerating voltage of 200 kV. STEM and STEM mapping were performed using a Talos F200X Atomic Resolution Analytical Microscope. TEM and STEM samples were prepared by casting a suspension of the materials on a carbon coated copper grid (300 mesh). XPS was carried out on a PHI Quantum 2000 spectrometer with multiprobe (Physical electronics industries Inc.) using Al Kα radiation (λ=1486.6eV) as the radiation source. The spectra of C 1s, N 1s, and Au 4f were collected and analyzed/fitted using Casa XPS software. Thermogravimetric analysis with mass spectroscopy (TGA-mass) was collected on a Dupont 951 thermogravimetric analyzer. During the test, the catalyst was first pretreated under Ar flow for 2 h at 200 °C. Then, 5% CO_2 in Ar was flow to the sample for 30 min at room temperature. The Ar flow was carried for 30 min to remove the physically adsorbed CO_2 before the TGA test from 27 °C to 600 °C with the ramp of 15 °C per min under Ar flow. The flow rates were all 50 mL min^{-1}. The mass spectrometry for CO_2 was collected during the TGA test. The gas products from CO_2 reduction were measured on a Shimadzu GC-2014 GC. The quantitative calculation of products was using the calibration curves built by the standard gas of CO and H_2. The liquid products were analyzed using ^{1}H NMR with DMSO as the internal standard on a Bruker Avance 400 MHz spectrometer. The water suppression method was used in each test. The soft X-ray absorption spectra at the N K-edge was performed at the REIXS beamline of the Canadian Light Source in partial fluorescence yield (PFY) mode. These measurements, sensitive to the unoccupied partial density of states of a particular element, are performed by exciting a core electron to the conduction band while monitoring the subsequent fluorescence decay. In a PFY measurement, the emitted photons are collected using an energy dispersive silicon drift detector, allowing the fluorescence associated with a particular core-hole transition of interest to be monitored. REIXS is an undulator beamline with a spot size of 60x10 μm^2 and the instrumental resolving power (E/ΔE) was approximately 4000. The spectra were normalized to the incoming photon flux using a gold mesh placed in the x-ray beam upstream of the sample and the energy axis was calibrated using an h-BN reference sample and an initial peak position of 402.10 eV. The N peaks were deconvoluted and the peak area was used to calculate the ratio of N sites.

Results and discussion

Sub-2 nm AuNCs supported on nitrided carbon (Au-2@CN) were prepared by the chemical reduction of $HAuCl_4$ on nitrided carbon as reported previously.[32-34] In brief, soft

nitriding of carbon (Printex U, Orion Co.) was carried out by annealing Printex U carbon with urea at 300 °C. After thoroughly washing to remove residual urea, nitrided carbon was dispersed in water together with $HAuCl_4$, followed by chemical reduction with $NaBH_4$ (see Experimental procedures for synthetic details). Scanning transmission electron microscopy (STEM) shows the growth of ultrasmall AuNCs on nitrided carbon (Figures 1a and b). Printex U carbon nanospheres have an average diameter of *ca.* 50 nm and the size of AuNCs is 1.9 ± 0.3 nm. AuNCs are highly dispersed on carbon (see more STEM images in Figure S2). The distribution of N sites and Au on carbon was confirmed by STEM energy-dispersive X-ray spectroscopy (Figure S2). The loading amount of AuNCs was estimated to be 2.5 wt% relative to carbon from thermogravimetric analysis (Figure S3), in consistence with the result from the STEM energy dispersive X-ray spectroscopy (Figure S2).

Electrochemical reduction of CO_2 was evaluated in 0.5 M $NaHCO_3$ aqueous solution (pH=7.2) using Au-2@CN in an "H" cell. The typical linear sweep voltammetry (LSV) is given in Figure 1c. Under N_2, only proton reduction occurred; when replaced with CO_2, much higher current density was seen which is indicative of high selectivity towards CO_2 reduction. The gas products were quantitatively analyzed in the potential window of -0.8 V to -0.28 V using gas chromatography (Figures 1d and S4-S10). H_2 and CO were confirmed as the two main gas products. A trace amount of formic acid can be detected from ^{1}H NMR as well (Figures S4-S10); but the FE for formic acid is <1%. Au-2@CN shows an onset potential of -0.28 V where CO can be detected as a gas product, corresponding to an overpotential of 174 mV, given $E(CO_2/CO)$ = -0.106 V. Au-2@CN gives a high FE for CO and a lower low FE for H_2 when the potential is lower than -0.45 V. At η = 544 mV, a mass activity (j_{CO}) of 721 A g^{-1} and a FE for CO of 89% are obtained, respectively (Figure 1d). A mass activity larger than 1000 A g^{-1} was achieved at -0.8 V, far better than the state-of-the-art Au-based nanocatalysts (Table S1) for CO_2 reduction.[19, 20, 22-27, 44, 45] We also confirmed that, the activity of CO_2 reduction originated from AuNCs other than the carbon support, since both activated carbon and nitrided carbon solely favored proton reduction in the potential range of -0.7 ~ -1.2 V (see Figures S11-S12). Note that, there are reports showing nitrided carbon as active catalysts for CO_2 reduction;[46-49] however, the nitrided carbon through soft nitriding is inactive for CO_2 reduction under conditions used in our studies. Using electrolyte with a lower concentration of $NaHCO_3$ (0.1 M) or higher loading of catalysts would lower the mass activity in CO_2 reduction (Table S2) since both the conductivity of the electrolyte and the difficulty of CO_2 diffusion through catalysts play key roles in determining the electroreduction.[50, 51]

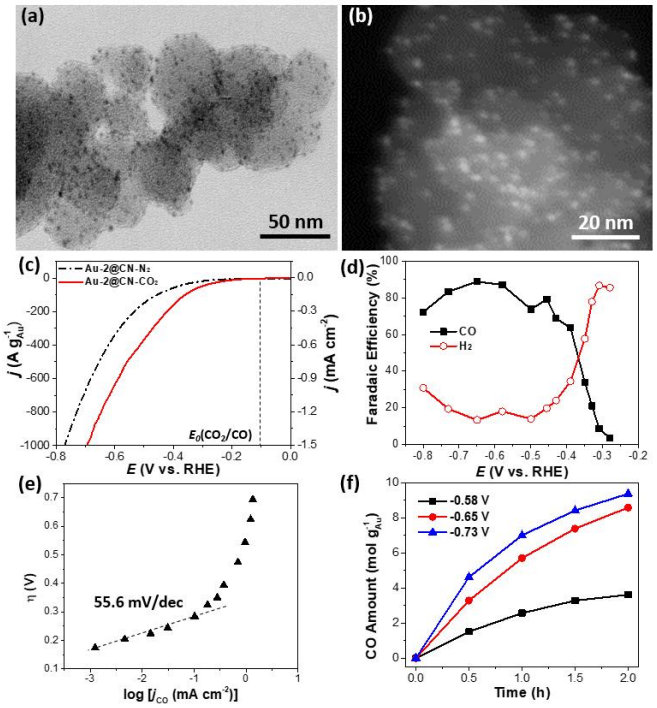

Figure 1. Electron microscopy of Au-2@CN and its CO_2 electrochemical reduction results. (a-b) Bright-field (a) and dark-field STEM images (b) of Au-2@CN. (c-f) LSV scans (c) of Au-2@CN at 10 mV s-1 in N2 (black, dash) and CO2 (red, solid) saturated $NaHCO_3$ solution (0.5 M). Faradaic efficiencies (d) for CO and H_2 at different potentials. Tafel plot (e) of Au-2@CN. CO production amount (f) using Au-2@CN at different potentials.

The kinetics of CO_2 reduction catalyzed by Au-2@CN was examined using a Tafel plot. The specific current density toward CO formation (j_{CO}) normalized to the electrochemical active surface area (ECSA) of Au was extracted from the total current density and CO FE. The plot of η *vs* log(j_{CO}) is displayed in Figure 1e. A Tafel slope of 55.6 mV dec^{-1} in the low overpotential region was seen and it is one of the lowest values compared to other reported values for CO_2 reduction using Au catalysts.[25, 27] The smaller Tafel slope is indicative of a fast electron transfer step prior to a rate-determining chemical step,[25, 52] which proves the formation of stable CO_2 intermediates on the surface of AuNCs.[27, 53, 54] Electron-rich AuNCs likely facilitate the electron transfer to CO_2 that thus enhances the activity of CO_2 reduction. The stability test of Au-2@CN was carried out at a constant potential for 2 h (Figure 1f). The rate of CO production is 2-7 mol h^{-1} per g_{Au} depending on the potential. The depression of CO production was seen after 1.5 h electrolysis which is likely caused by the increase in the size of AuNCs. After 2 h electrolysis, the average size of AuNCs increased to 3.8 ± 0.6 nm as examined by TEM (see Figure S13). This agrees with the drop in the ECSA of Au by 77% (Figure S13). The low stability of AuNCs is due to large surface energy similar to other nanocatalysts reported in literature.[31, 55] The durability of AuNCs in CO_2 reduction is still an obstacle for the practical use of our catalysts.

DFT calculation was applied to estimate the free energy of each steps in the catalytic process using electron-rich and neutral Au_{28} clusters in order to understand the influence of Au surface charge density on CO_2 reduction. This model has been used in our previous simulation for selective oxidation.[32] The CO_2 reduction on Au is simply assumed to include the following steps for the two-electron CO_2 reduction:[22]

$$CO_2 + H^+ + e^- + * \rightarrow COOH^* \quad (1)$$

$$COOH^* + H^+ + e^- \rightarrow CO^* + H_2O \quad (2)$$

$$CO^* \rightarrow CO + * \quad (3)$$

Figure S14 displays the calculated free energy diagram for CO_2 reduction on Au_{28} clusters basing on the computational hydrogen electrode (CHE) model.[56] One CO_2 and a proton-electron pair adsorbed on a Au_{28} cluster to first form a carboxyl intermediate (COOH*); then, the COOH* intermediate can dissociate into CO* and H_2O as products by adding the second proton-electron pair. On the neutral cluster, the CO_2 activation through COOH* formation was associated with a free energy of 0.68 eV. While on the electron-rich cluster, the formation of the COOH* intermediate has a significantly lower free energy barrier of 0.42 eV. As such, electron-rich AuNCs likely favor the reduction of CO_2.

However, electron-rich Au_{28} clusters also showed much lower activation energy for proton reduction. The CHE model indicated that the free energy change (ΔG) to form the H* intermediate on electron-rich clusters is 0.26 eV, lower than that on the neutral cluster, 0.53 eV (Figure S14). The DFT results agreed that AuNCs with smaller sizes favor proton reduction as reported previously.[22, 30] Since electron-rich Au catalysts and nitrided carbon do not solely promote CO_2 reduction, we further investigate the cooperative effect of AuNCs and N sites on nitrided carbon support.

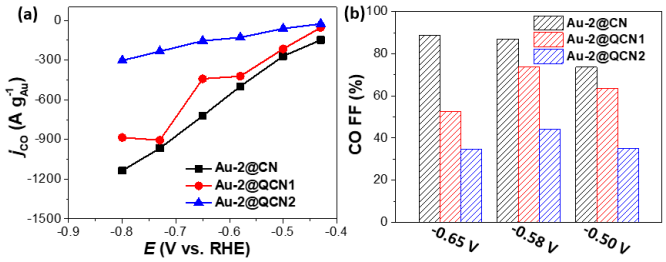

Figure 2. The effect of nitrogen sites on electrochemical reduction of CO_2. Mass activity (a) and CO FE (b) of Au-2@CN, Au-2@QCN1 and Au-2@QCN2 at different potentials

To gain further insight into the role of N sites on electrochemical reduction of CO_2, two reactions were used to selectively quench N sites. Carbylamine reaction is known to terminate primary amines with $CHCl_3$ in the presence of bases[57], and alkylation with chloroethanol is known to react all amines to form quaternary ammonium salt.[58] Both reactions were carried out under mild conditions which had slight impacts on the size and the ECSA of AuNCs (Figures S15-S16). Au-2@QCN1 and Au-2@QCN2 denote the samples quenched by $CHCl_3$ and chloroethanol, respectively. CO_2 reduction using these two catalysts was examined under identical reaction conditions as descried for Au-2@CN. Figure 2a gives the plot of j_{CO} of Au catalysts before and after quenching N sites. The activity for CO_2 reduction shows a ~10% and ~75% decrease for Au-2@QCN1 and Au-2@QCN2, respectively, compared to that of Au-2@CN. The CO FE of Au-2@QCN2 is only 30-40% in the potential window of -0.4 V to -0.8 V (Figures 2b and S15-S16), close to the reported values from Cuenya[30] and Jin[24].

X-ray photoelectron spectroscopy (XPS) was used to investigate the change in electronic states of Au and N along quenching nitrogen sites. Au-2@CN shows two asymmetric peaks at 83.9 eV and 87.6 eV, assigning to the binding energy of Au 4f (Figure 3c). The quenching of surface nitrogen sites on carbon resulted in a gradual shift of Au 4f peaks. After alkylation of amines, the binding energy of Au 4f $_{7/2}$ shifted to 84.2 eV. The increase in the binding energy of Au 4f peaks suggests that the surface of AuNCs became electron-deficient after quenching nitrogen sites. On the other hand, the binding energy of N 1s had a 0.4 eV decrease from 400 eV for Au-2@CN to 399.6 eV for both Au-2@QCN1 and Au-2@QCN2. Surface nitrogen sites on nitrided carbon contain three main N species, including amine and amide groups (~400 eV), quaternary nitrogen (or graphitic, ~401.1 eV) and pyridinic nitrogen (~398.6 eV).[34] The fitting curves show that the graphitic nitrogen gradually dropped from 14.9% for Au-2@CN to 7.0% for Au-2@QCN1 and 3.5% for Au-2@QCN2. The removal of surface graphitic nitrogen sites obviously changed the electronic interaction of AuNCs and nitrided carbon support in the course of quenching reactions,[59] although the exact reaction mechanism is unclear currently. In addition, we utilized N K-edge X-ray absorption spectroscopy (XAS) to confirm the evolution of N sites along quenching experiments (see FigureS 3c, 3d and Figure S17). The N K-edge consists of three main absorption peaks at 398.9 eV, 400.2 eV and 401.4 eV designating as pyridinic N (N1), ureido (or amide) (N2), and graphitic N (N3), respectively. The decrease in pyridinic and graphitic N sites was observed similar to the XPS results. Interestingly, a clear shoulder peak at ~399.2 eV is seen for Au-2@CN that can be assigned to metal-N binding.[60, 61] The disappearance of this feature after quenching N sites is also an evidential sign to the weakened metal-N interaction. Those findings show that the quenching of N sites results in the decrease in surface charge density of AuNCs (or the Au-carbon electronic effect) and electron-deficient AuNCs are less selective catalysts for CO_2 reduction.

Nanoscale

ARTICLE

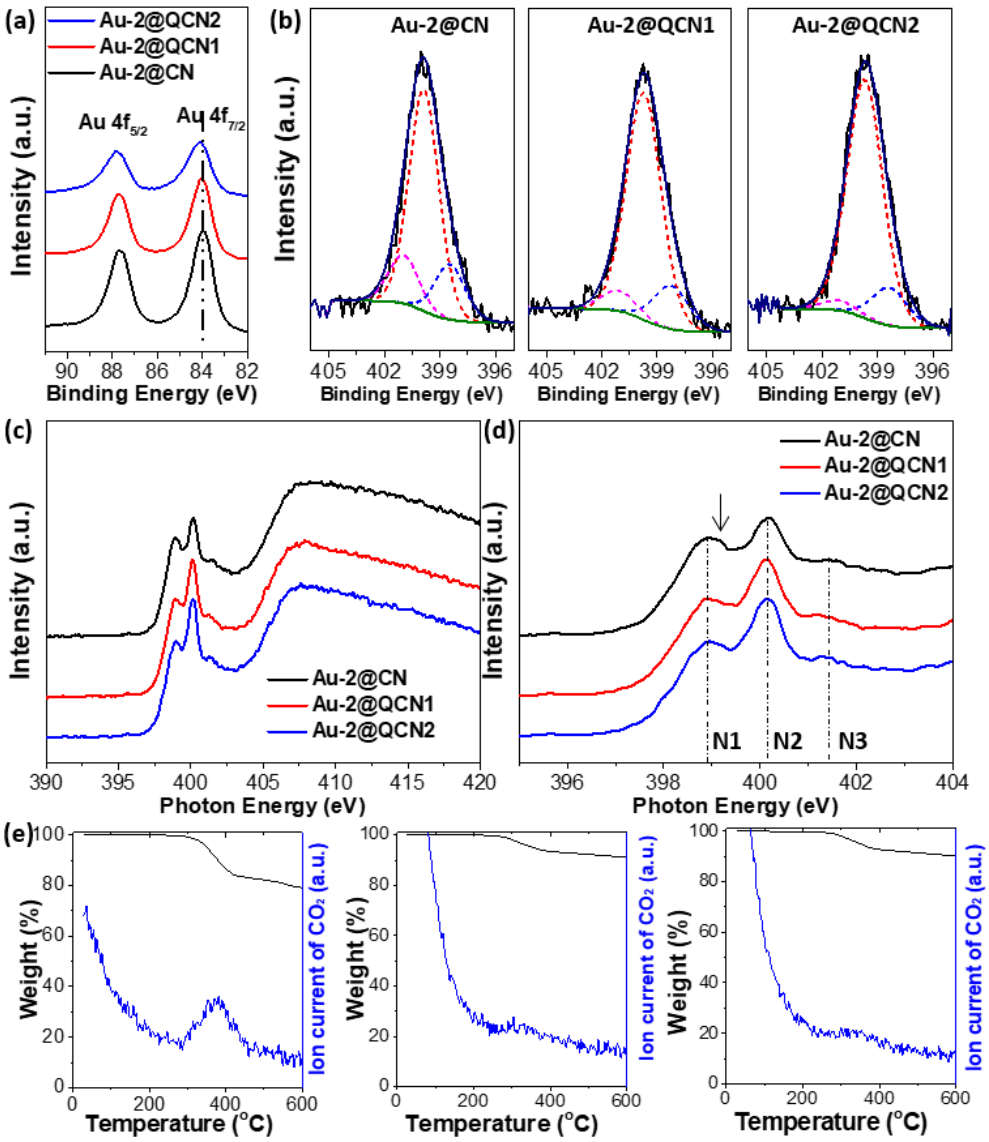

Figure 3. Surface characterization of catalysts. XPS spectra of Au 4f (a) and N 1s (b), N K-edge XAS spectra (c,d) of Au-2@CN, Au-2@QCN1 and Au-2@QCN2; (e) TGA-MS results for CO_2 desorption of Au-2-CN (left), Au-2@QCN1 (middle) and Au-2@QCN2 (right).

Other than the electronic effect on AuNCs, various nitrogen sites (*e.g.* amine, pyridine and graphitic N) on carbon supports can interact with CO_2 through acid-base chemisorption. We probed the potential adsorption of CO_2 on Au-2@CN, Au-2@QCN1 and Au-2@QCN2 using thermogravimetric analysis with a mass spectrometer (TGA-MS, see Experimental procedures for the details). Figure 3e shows that Au-2@CN showed a strong CO_2 desorption peak at *ca.* 380 °C; while, a very weak CO_2 signal could be seen for Au-2@QCN1 and Au-2@QCN2. This suggests that the two catalysts after quenching N sites did not show obvious CO_2 desorption. The adsorption of CO_2 obviously occurred on the surface N sites since the desorption occurred at decomposition of nitrided carbon. The two catalysts after quenching N sites showed less mass loss, which is caused by the loss of some N species during the reactions (Figure S18). We also did not see CO_2 adsorption on pristine Printex U carbon (see Figure S19). The adsorbed CO_2 on nitrided carbon can kinetically promote

CO_2 reduction through the increase of localized CO_2 concentration. The primary amines, however, are less likely involved in the cooperative effect because Au-2@QCN1 shows close activity as Au-2@CN. We emphasize that, the catalytic enhancement for CO_2 reduction arises from the cooperative effect, *i.e.*, the electronic states of Au and the basicity of the surface nitrogen sites. However, the surface nitrogen sites solely are inactive for CO_2 reduction as shown in our control experiments when using nitrided carbon as catalysts.

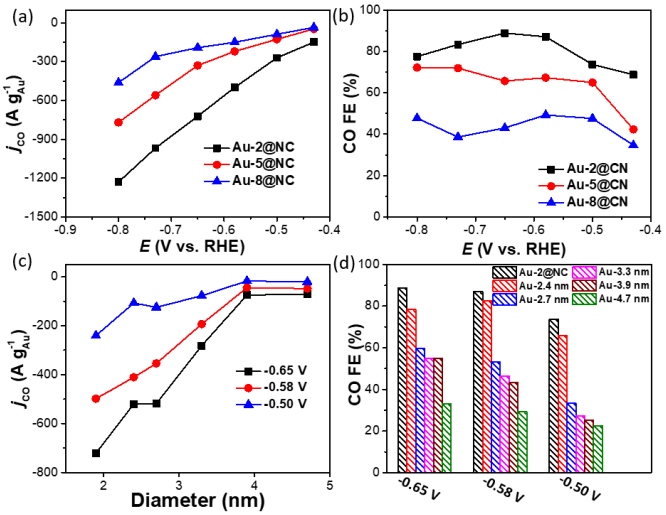

Figure 4. Size effect of AuCNs on electrochemical reduction of CO_2. Mass activity (a) and CO FE (b) of Au-2@CN, Au-5@CN and Au-8@CN synthesized using one-step chemical reduction; Mass activity (c) and CO FE (d) of AuNCs synthesized via seed-mediated growth using Au-2@CN as seeds.

The Au-support electronic interaction is known to be size-dependent.[32] Larger AuNCs grown on nitrided carbon has proven to be less electron-rich, compared to Au-2@CN. To assess the size effect of Au, we designed two experiments to grow AuNCs having different sizes ranged 2-8 nm. First, ligand-free AuNCs with similar loading mass but different average diameters of 5.1 nm and 8.4 nm were grown on nitrided carbon by varying the solution pH (denoted as Au-5@CN and Au-8@CN, Figure S20).[34] The mass activity toward CO_2 reduction and CO FE were summarized in Figure 4a and b. Au-5@CN and Au-8@CN are less active for CO_2 reduction, though the activity difference in their LSV scans are minimum (Figure S21). At -0.8 V, Au-2@CN showed a j_{CO} of -1200 A g_{Au}^{-1}, which is 1.5 times and 2.5 times higher than that of Au-5@CN and Au-8@CN, respectively. In the potential window of -0.4 V to -0.8 V, the CO FE of ~70 % and ~45 % were seen for Au-5@CN and Au-8@CN, respectively. Second, we prepared AuNCs with an average size of 2.4-4.7 nm supported on nitrided carbon using Au-2@CN as seeds via the seed-mediated growth (Figure S22, see Experimental procedures for details). The j_{CO} and the selectivity of CO_2 reduction dropped dramatically even slightly increasing the size of AuNCs (Figure 4c-d). At -0.65 V (vs RHE), j_{CO} decreased from 721 A g-1 to 71.8 A g-1 and CO FE decreased from 88.8% to 54.9% when the size of AuNCs increased from 1.9 nm to 4.7 nm. Those results therefore confirm that the electronic interaction of Au-carbon played a key role in determining the selectivity of CO_2 reduction over water reduction.

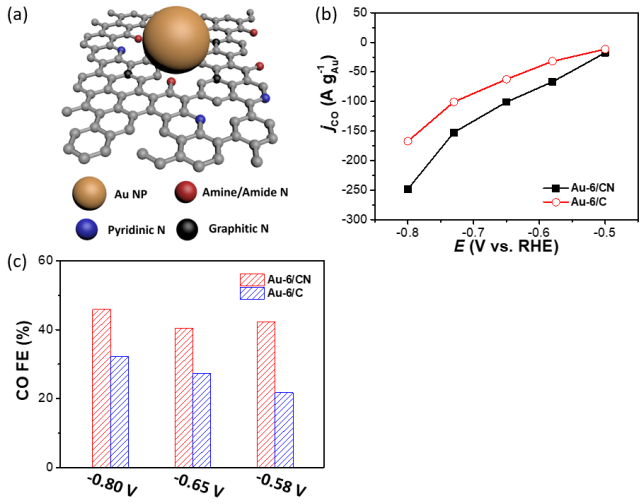

Figure 5. Electrochemical CO_2 reduction of AuNCs adsorbed on CN and C. (a) Scheme of CO_2 reduction on Au@CN; Mass activity (b) and CO FE (c) using Au-6/CN and Au-6/C at different potentials.

We further investigated whether we can use the cooperative catalytic effect of the nitrided carbon and AuNCs universally. Au NPs with an average size of 6.8 nm were prepared using oleylamine as ligands.[41, 42] Those Au NPs were then adsorbed physically on nitrided carbon and pristine carbon (Figures S23-S24). The two Au NPs were studied for CO_2 reduction under identical conditions. Au NPs on nitrided carbon showed a higher mass activity toward CO_2 reduction, compared to that of Au NPs supported on pristine carbon (Figure 5b). At -0.58 V, 2 times higher mass activity and CO FE were received for Au NPs on nitrided carbon, compared to the same AuNPs loaded on activated carbon.

Conclusions

In the aqueous-phase electrochemical reduction of CO_2, there are many literatures suggesting that ultrasmall Au catalysts with sub-2 nm favors to reduce water over CO_2.[24, 30, 31] Our observation is that the 1.9 nm AuNCs supported on nitrided carbon are highly selective and active in CO_2 reduction. Au-2@CN exhibited a low onset potential of -0.28 V and a high FE (> 80%) for CO when the potential is lower than -0.45 V in 0.5 M $NaHCO_3$ aqueous solution. The mass activity of Au-2@CN reached > 1000 A g^{-1} at -0.8 V, that is an order of magnitude higher than many state-of-the-art Au-based nanocatalysts.[19, 20, 22-27, 44, 45] The N sites on the nitrided carbon have proven to be critical in control of the selectivity of CO_2 reduction. After quenching the N sites, an obvious drop of CO FE and mass activity was seen (see Figure 3). The effects of N sites on CO_2 reduction are two-fold. First, the N sites acting as Lewis base improve the localized concentration of CO_2 nearby catalytically active Au by chemisorption. TGA-MS

results confirm that the nitrided carbon has a strong CO_2 chemisorption compared to the ones with quenched N sites. The activity for CO_2 reduction showed a ~75% drop and the CO FE decreased by 50% for Au-2@QCN2 in the absence of N sites, compared to that of Au-2@CN. Second, the N sites enriching the surface charge density of AuNCs likely favors the binding of CO_2, as demonstrated by high-resolution XPS results, DFT and the size effect of Au catalysts on the CO_2 reduction selectivity. When increasing the size of Au catalysts, the CO FE decreased in two independent controls that demonstrated the importance of Au-support electronic interaction. The preferential reduction of CO_2 over water using ultrasmall AuNCs is thus originated for the cooperative catalytic effect of the nitrided carbon and AuNCs. We further showed that the Au-carbon interaction can be applied to other pre-synthesized Au NPs to promote the catalytic activity and selectivity for CO_2 reduction. However, the low stability is still unresolved in our current study that limits the practical use of AuNCs in CO_2 reduction. More efforts are needed to stabilize Au catalysts while maintaining their high mass activity and selectivity.

Acknowledgements

This work is supported in part through the National Science Foundation (CBET #1705566). The SEM/TEM studies were performed using the facilities in the UConn/FEI Center for Advanced Microscopy and Materials Analysis (CAMMA). This work was also partially supported by the Green Emulsions Micelles and Surfactants (GEMS) Center. The XAS measurements are supported by the Natural Sciences and Engineering Research Council of Canada (NSERC) and the Canada Research Chairs program.

Notes and references

1. J. Qiao, Y. Liu, F. Hong and J. Zhang, *Chem. Soc. Rev.*, 2014, **43**, 631-675.
2. D. T. Whipple and P. J. A. Kenis, *J. Phys. Chem. Lett.*, 2010, **1**, 3451-3458.
3. N. S. Lewis and D. G. Nocera, *PNAS*, 2006, **103**, 15729-15735.
4. B. P. Sullivan, K. Krist and H. Guard, *Electrochemical and electrocatalytic reactions of carbon dioxide*, Elsevier, 2012.
5. B. Kumar, M. Llorente, J. Froehlich, T. Dang, A. Sathrum and C. P. Kubiak, *Ann. Rev. Phys. Chem.*, 2012, **63**, 541-569.
6. W. Wang, S. Wang, X. Ma and J. Gong, *Chem. Soc. Rev.*, 2011, **40**, 3703-3727.
7. J. Schneider, H. Jia, J. T. Muckerman and E. Fujita, *Chem. Soc. Rev.*, 2012, **41**, 2036-2051.
8. X. Chang, T. Wang and J. Gong, *Energy Environ. Sci.*, 2016, **9**, 2177-2196.
9. C. Costentin, M. Robert and J.-M. Savéant, *Chem. Soc. Rev.*, 2013, **42**, 2423-2436.
10. S. Ma, Y. Lan, G. M. Perez, S. Moniri and P. J. Kenis, *ChemSusChem*, 2014, **7**, 866-874.
11. M. Ma, B. J. Trześniewski, J. Xie and W. A. Smith, *Angew. Chem. Int. Ed.*, 2016, **55**, 9748-9752.
12. S. Rasul, D. H. Anjum, A. Jedidi, Y. Minenkov, L. Cavallo and K. Takanabe, *Angew. Chem.*, 2015, **127**, 2174-2178.
13. D. Raciti, K. J. Livi and C. Wang, *Nano lett.*, 2015, **15**, 6829-6835.
14. D. Gao, H. Zhou, J. Wang, S. Miao, F. Yang, G. Wang, J. Wang and X. Bao, *J. Am. Chem. Soc.*, 2015, **137**, 4288-4291.
15. S. Back, M. S. Yeom and Y. Jung, *Acs Catal*, 2015, **5**, 5089-5096.
16. E. R. Cave, J. H. Montoya, K. P. Kuhl, D. N. Abram, T. Hatsukade, C. Shi, C. Hahn, J. K. Norskov and T. F. Jaramillo, *Phys. Chem. Chem. Phys.*, 2017, **19**, 15856-15863.
17. P. Christensen, A. Hamnett, A. Muir and N. Freeman, *J. Electroanal. Chem. Interfacial Electrochem.*, 1990, **288**, 197-215.
18. E. B. Nursanto, H. S. Jeon, C. Kim, M. S. Jee, J. H. Koh, Y. J. Hwang and B. K. Min, *Catal. Today*, 2016, **260**, 107-111.
19. T. N. Huan, P. Prakash, P. Simon, G. Rousse, X. Xu, V. Artero, E. Gravel, E. Doris and M. Fontecave, *ChemSusChem*, 2016, **9**, 2317-2320.
20. C. Rogers, W. S. Perkins, G. Veber, T. E. Williams, R. R. Cloke and F. R. Fischer, *J. Am. Chem. Soc.*, 2017, **139**, 4052-4061.
21. Y. Hori, K. Kikuchi and S. Suzuki, *Chem. Lett.*, 1985, **14**, 1695-1698.
22. W. Zhu, R. Michalsky, Ö. Metin, H. Lv, S. Guo, C. J. Wright, X. Sun, A. A. Peterson and S. Sun, *J. Am. Chem. Soc.*, 2013, **135**, 16833-16836.
23. W. Zhu, Y.-J. Zhang, H. Zhang, H. Lv, Q. Li, R. Michalsky, A. A. Peterson and S. Sun, *J. Am. Chem. Soc.*, 2014, **136**, 16132-16135.
24. D. R. Kauffman, D. Alfonso, C. Matranga, H. Qian and R. Jin, *J. Am. Chem. Soc.*, 2012, **134**, 10237-10243.
25. Y. Chen, C. W. Li and M. W. Kanan, *J. Am. Chem. Soc.*, 2012, **134**, 19969-19972.
26. D. Gao, Y. Zhang, Z. Zhou, F. Cai, X. Zhao, W. Huang, Y. Li, J. Zhu, P. Liu and F. Yang, *J. Am. Chem. Soc.*, 2017, **139**, 5652-5655.
27. Z. Cao, D. Kim, D. Hong, Y. Yu, J. Xu, S. Lin, X. Wen, E. M. Nichols, K. Jeong, J. A. Reimer, P. Yang and C. J. Chang, *J. Am. Chem. Soc.*, 2016, **138**, 8120-8125.
28. M. Liu, Y. Pang, B. Zhang, P. De Luna, O. Voznyy, J. Xu, X. Zheng, C. T. Dinh, F. Fan, C. Cao, F. P. G. de Arquer, T. S. Safaei, A. Mepham, A. Klinkova, E. Kumacheva, T. Filleter, D. Sinton, S. O. Kelley and E. H. Sargent, *Nature*, 2016, **537**, 382-386.
29. G. A. Olah, G. K. S. Prakash and A. Goeppert, *J. Am. Chem. Soc.*, 2011, **133**, 12881-12898.
30. H. Mistry, R. Reske, Z. Zeng, Z.-J. Zhao, J. Greeley, P. Strasser and B. R. Cuenya, *J Am Chem Soc*, 2014, **136**, 16473-16476.
31. J. A. Trindell, J. Clausmeyer and R. M. Crooks, *J. Am. Chem. Soc.*, 2017, **139**, 16161-16167.
32. B. Liu, P. Wang, A. Lopes, L. Jin, W. Zhong, Y. Pei, S. L. Suib and J. He, *ACS Catal.*, 2017, **7**, 3483-3488.
33. H. Yao, B. Liu, I. M. Mosa, I. Bist, J. He and J. F. Rusling, *ChemElectroChem*, 2016, **3**, 2100-2109.
34. B. Liu, H. Yao, W. Song, L. Jin, I. M. Mosa, J. F. Rusling, S. L. Suib and J. He, *J. Am. Chem. Soc.*, 2016, **138**, 4718-4721.
35. C. Kim, T. Eom, M. S. Jee, H. Jung, H. Kim, B. K. Min and Y. J. Hwang, *ACS Catal.*, 2016, **7**, 779-785.

36. H. Coskun, A. Aljabour, P. De Luna, D. Farka, T. Greunz, D. Stifter, M. Kus, X. Zheng, M. Liu and A. W. Hassel, *Sci. Adv.*, 2017, **3**, e1700686.
37. Y. Fang and J. C. Flake, *J. Am. Chem. Soc.*, 2017, **139**, 3399-3405.
38. H. Sakurai and M. Haruta, *Catal. Today*, 1996, **29**, 361-365.
39. K. Teramura, T. Tanaka, H. Ishikawa, Y. Kohno and T. Funabiki, *J. Phys. Chem. B*, 2004, **108**, 346-354.
40. Y. Yang, L. Jin, B. Liu, P. Kerns and J. He, *Electrochimica Acta*, 2018, **269**, 441-451.
41. S. Peng, Y. Lee, C. Wang, H. Yin, S. Dai and S. Sun, *Nano Res.*, 2008, **1**, 229-234.
42. O. K. Ranasingha, C. Wang, P. R. Ohodnicki, J. W. Lekse, J. P. Lewis and C. Matranga, *J. Mater. Chem. A*, 2015, **3**, 15141-15147.
43. A. Sukeri, L. P. H. Saravia and M. Bertotti, *Phys. Chem. Chem. Phys.*, 2015, **17**, 28510-28514.
44. X. Feng, K. Jiang, S. Fan and M. W. Kanan, *J. Am. Chem. Soc.*, 2015, **137**, 4606-4609.
45. H.-E. Lee, K. D. Yang, S. M. Yoon, H.-Y. Ahn, Y. Y. Lee, H. Chang, D. H. Jeong, Y.-S. Lee, M. Y. Kim and K. T. Nam, *ACS Nano*, 2015, **9**, 8384-8393.
46. H.-R. M. Jhong, C. E. Tornow, B. Smid, A. A. Gewirth, S. M. Lyth and P. J. A. Kenis, *ChemSusChem*, 2017, **10**, 1094-1099.
47. P. Xia, B. Zhu, J. Yu, S. Cao and M. Jaroniec, *J. Mater. Chem. A*, 2017, **5**, 3230-3238.
48. J. Lin, Z. Pan and X. Wang, *ACS Sustain. Chem. Eng.*, 2014, **2**, 353-358.
49. X. Lu, T. H. Tan, Y. H. Ng and R. Amal, *Chem. Eur. J.*, 2016, **22**, 11991-11996.
50. X. Min and M. W. Kanan, *J. Am. Chem. Soc.*, 2015, **137**, 4701-4708.
51. S. Verma, X. Lu, S. Ma, R. I. Masel and P. J. A. Kenis, *Phys. Chem. Chem. Phys.*, 2016, **18**, 7075-7084.
52. Y. Chen and M. W. Kanan, *J. Am. Chem. Soc.*, 2012, **134**, 1986-1989.
53. Y.-C. Hsieh, S. D. Senanayake, Y. Zhang, W. Xu and D. E. Polyansky, *ACS Catal.*, 2015, **5**, 5349-5356.
54. Q. Lu, J. Rosen, Y. Zhou, G. S. Hutchings, Y. C. Kimmel, J. G. Chen and F. Jiao, *Nat. Commun.*, 2014, **5**, 3242.
55. G. Jun, H. Florent, L. Jeremy and H. Xile, *Angew. Chem.*, 2018, **130**, 2993-2997.
56. A. A. Peterson, F. Abild-Pedersen, F. Studt, J. Rossmeisl and J. K. Norskov, *Energy Environ. Sci.*, 2010, **3**, 1311-1315.
57. P. A. SMITH and N. W. KALENDA, *J. Org. Chem.*, 1958, **23**, 1599-1603.
58. S.-W. Lin, Q. Sun, Z.-M. Ge, X. Wang, J. Ye and R.-T. Li, *Bioorg. Med. Chem. Lett.*, 2011, **21**, 940-943.
59. X. Ning, H. Yu, F. Peng and H. Wang, *J. Catal.*, 2015, **325**, 136-144.
60. J. Zhou, P. N. Duchesne, Y. Hu, J. Wang, P. Zhang, Y. Li, T. Regier and H. Dai, *Phys. Chem. Chem. Phys.*, 2014, **16**, 15787-15791.
61. P. Chen, T. Zhou, L. Xing, K. Xu, Y. Tong, H. Xie, L. Zhang, W. Yan, W. Chu, C. Wu and Y. Xie, *Angew. Chem. Int. Ed.*, 2017, **56**, 610-614.

Table of Contents

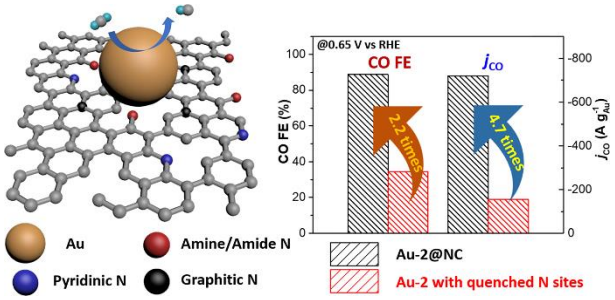

Ultrasmall Au nanocatalysts supported on nitrided carbon show superior mass activity and high selectivity for CO_2 electrochemical reduction as a results of the synergy of surface nitrogen sites of carbon and electron-rich Au surface.